An Efficient Multichannel SAR Channel Phase Error Calibration Method Based on Fine-Focused HRWS SAR Image Entropy

Jixiang Xiang, *Member, IEEE*, Xiaojie Ding, *Member, IEEE*, Guang-Cai Sun, *Senior Member, IEEE*, Zijing Zhang, *Member, IEEE*, Mengdao Xing, *Fellow, IEEE*, and Wenkang Liu, *Member, IEEE*

***Abstract*—Azimuth multichannel synthetic aperture radar (SAR) is a useful approach to solving minimum antenna area constraint and realizing high resolution and wide swath (HRWS) imaging by multichannel signal reconstruction. However, channel phase error will significantly degrade the reconstruction performance and leads to azimuth ghost. This article presents an efficient minimum entropy channel error estimation method based on fine-focused SAR image. The multichannel SAR images are obtained by using Range-Doppler imaging algorithm applied for preprocessed data of each channel. Then, the reconstruction and the residual range cell migration and residual second range compression compensation are performed to achieve multichannel fine-focused SAR images. After overlapping these multichannel fine-focused SAR images and iteratively calibrating the channel phase error, fine-focused HRWS SAR image can be achieved. Therefore, the SAR image used in the channel error estimation process can directly obtain the fine focused HRWS SAR image after minimum entropy iteration without additional imaging operations. Compared with the minimum entropy method by using the coarse-focused SAR image based on azimuth deramp, redundant reconstruction, and imaging operations are avoided. Thus, error estimation and imaging processing procedures are optimized. Processing efficiency improvement are analyzed, and simulation and acquired data processing verify the effectiveness of the proposed method.**

***Index Terms*—Azimuth multichannel synthetic aperture radar (SAR), channel phase error estimation, image domain, minimum entropy.**

I. Introduction

DUE to the limitation of minimum antenna area constraint, traditional single-channel synthetic aperture radar (SAR) [1], [2], [3], [4] systems cannot simultaneously achieve high resolution and wide swath (HRWS) imaging [4], [5], [6], [7], [8], [9], [10], [11], [12], [13]. Combined with digital beamforming (DBF) technology [13], [14], [15], [16], the proposal of azimuth channel SAR effectively solves the basic contradiction between low-azimuth spatial sampling and high azimuth resolution, which limits the "minimum antenna area" of single-channel SAR. The azimuth multichannel SAR system works at a lower azimuth sampling frequency, i.e., pulse repetition frequency (PRF), and sets up multiple receiving channels along the moving route of the radar platform. Essentially, the system increases the azimuth temporal sampling rate (i.e., PRF) of the system equivalently by increasing the spatial sampling of the system orientation. Since the actual working PRF of the SAR system is less than the Nyquist sampling frequency of each channel, according to the sampling theorem, we know that the echoes received by each channel are undersampled in the azimuth direction, which is reflected in the multichannel The azimuth spectrum of SAR data is folded, which will cause serious azimuth ambiguity in the final imaging result. Therefore, the classical multichannel SAR imaging processing method needs to reconstruct the multichannel data before imaging the multichannel data. Typical methods include DBF, space-time adaptive processing [16], [17], [18], and system function inversion methods [19], [20]. After reconstruction, the multichannel SAR data can be equivalent to a single channel, and then various classical time-domain and frequency-domain imaging algorithms can be used to perform imaging focusing processing of the SAR data [21], [22], [23], [24], [25].

However, in practice, channel mismatches inevitably exist due to phase gain errors, location uncertainty, and timing uncertainty between channels. The channel mismatch will seriously affect the reconstruction performance, resulting in the presence of azimuthal ambiguity (i.e., ghosts) in the SAR images, which will seriously reduce the SAR image quality. Therefore, estimation and correction for the mismatch between channels in multichannel SAR becomes a key problem in practical operation. Aiming at the channel mismatch in azimuth multichannel HRWS SAR, especially the phase error between channels, most of the existing methods perform estimation and compensation in the frequency domain, and some methods use image quality, such as, image entropy and other image evaluation measures, to iteratively adjust the channels with channel phase errors.

Manuscript received 27 June 2022; revised 17 August 2022; accepted 28 August 2022. Date of publication 13 September 2022; date of current version 21 September 2022. This work was supported in part by the State Key Program of National Natural Science of China under Grant 61931025, in part by the National Natural Science Foundation of China under Grant 62222113 and Grant 62101404, and in part by the National Science Fund for Distinguished Young Scholars under Grant 61825105. *(Xiaojie Ding contributed equally to this work.) (Corresponding authors: Guang-Cai Sun; Wenkang Liu.)*

Jixiang Xiang, Xiaojie Ding, Guang-Cai Sun, Zijing Zhang, and Mengdao Xing are with the National Laboratory of Radar Signal Processing, Xidian University, Xi'an 710071, China, and also with the Collaborative Innovation Center of Information Sensing and Understanding, Xidian University, Xi'an 710071, China (e-mail: jx_xiang@foxmail.com; xj_ding0719@163.com; rsandsgc@126.com; zjzhang@xidian.edu.cn; xmd@xidian.edu.cn).

Wenkang Liu is with the Academy of Advanced Interdisciplinary Research, Xidian University, Xian 710071, China (e-mail: wkliu@stu.xidian.edu.cn).

Digital Object Identifier 10.1109/JSTARS.2022.3206355

The signal subspace (SSP) channel error estimation method based on multichannel data [26] can be used to estimate the channel phase error in a distributed small satellite SAR system or an azimuth multichannel SAR system, but the method does not consider the spatial variability of the phase error. To improve this issue, Zhang et al. [27] proposed a two-step correction-based channel error correction algorithm based on SSP, including coarse correction and fine correction. The previous step corrects for range sampling time errors, constant amplitude and phase errors, and antenna position errors; while fine corrections correct for residual constant phase errors, baseline measurement errors, and phase errors for range-varying channels. This kind of subspace-based method estimates the channel error based on the orthogonality of the signal subspace and the noise subspace. Thus, the multichannel SAR system requires redundant spatial degrees of freedom to construct the noise subspace. That is, the number of channels is required to be greater than the azimuth ambiguity number of the SAR data. This feature limits the application of such signal subspace-based error estimation methods in practical processing.

The methods based on image quality evaluation have no requirement for redundant spatial degrees of freedom, which means this type of methods have a wider application range in practice. Sun et al. [28], for the Gaofen-3 dual-channel SAR data, proposed a channel phase error correction method based on quality factor, which optimized the image quality factor through heuristic iterative, and realized the problem of lack of degrees of freedom. An estimate of the channel error in the case. However, this scheme is only applicable to the dual-channel SAR system such as Gaofen-3, and the situation of more channels is still to be studied. Zhang et al. [29] proposed a channel error correction method based on weighted minimum entropy (WME) and local maximum likelihood (LML). This method uses the WME method to estimate the phase error of the coarsely focused image and uses the LML to estimate the range variant phase error. However, the image evaluated by the entropy value of this method is a two-dimensional (2-D) coarsely focused SAR image based on the azimuth deramp, and the coarsely focused image used cannot directly obtain the ambiguity-free SAR image. Thus, an additional imaging processing is required.

This article presents an efficient minimum entropy channel error estimation method based on fine-focused SAR image. First, the multichannel data are aligned in the azimuth direction by preprocessing operation. The multichannel SAR images are obtained by using Range-Doppler imaging algorithm with correcting range cell migration (RCM) in the frequency domain [30], [31], [32]. Then, the reconstruction factor multiplying and the residual RCM and residual second range compression (rSRC) compensation are performed to achieve multichannel fine-focused SAR images. After overlapping these multichannel fine-focused SAR images and iteratively calibrating the channel phase error by minimizing the fine-focused entropy, fine-focused HRWS SAR Image can be achieved. Thus, the SAR images used in the channel error estimation process can directly produces the fine focused HRWS SAR image after minimum entropy iteration, without additional imaging operations. The channel phase error estimation and imaging processing procedures are optimized. Compared with the minimum entropy method based on the coarse-focused SAR image in [29], redundant reconstruction and imaging operations are avoided, which promotes the efficiency of signal processing. Processing efficiency improvement are quantitatively analyzed in this article.

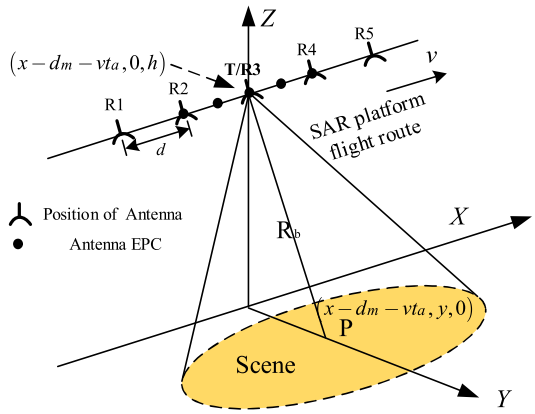

Fig. 1. Imaging geometry of azimuth multichannel SAR.

The rest of this article is organized as follow. The signal model and preprocessing are introduced in Section II. In Section III, the proposed method is presented in detail, including multichannel SAR imaging and reconstruction in Section III-A and fine-focused SAR entropy definition and procedure of the proposed method. In Section IV, computational complexity of the proposed method is analyzed, and the improvement in computational complexity is evaluated compared with the traditional ME. Section V shows the processing and analysis results of simulated and acquired multichannel SAR data. Finally, Section VI concludes this article.

II. Signal Model and Preprocessing

Fig. 1 shows a typical imaging geometric model of an azimuth multichannel SAR system. As shown in Fig. 1, the antennas of the multichannel SAR system are distributed along the direction of the radar trajectory. The antenna channel located at the center of the antenna array transmits a chirp signal (LFM, or chirp signal), and all antenna channels can receive the echo signal of the scene. According to the principle of equivalent phase center, the radar echo of the separate transmitting and receiving antennas is equivalent to the radar at the center of the transmitting antenna and the receiving antenna after the equivalent phase center error compensation.

In the system shown in Fig. 1, the internal of adjacent two channels is d. According to this principle, the internal of two adjacent equivalent phase centers (shown as black dots in Fig. 1) is $d/2$. The distance between mth channel and the reference channel is $d_m = (m-(M+1)/2)d/2$, where $m = 1,2,\ldots,M$, M denotes the number of channels. The multichannel SAR platform flies along the radar trajectory at a speed v. For the convenience of formula derivation, the radar works in the side-looking mode. P is the central point of the imaging scene. The range fast time and azimuth slow time are represented by t_r and t_a, respectively.

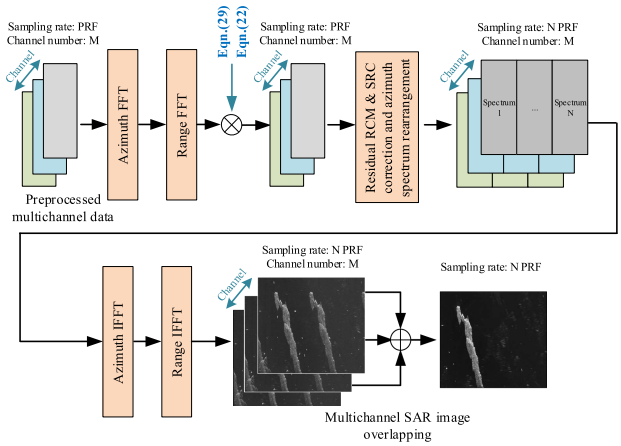

Fig. 2. The Processing flowchart for the ambiguity-free HRWS SAR image.

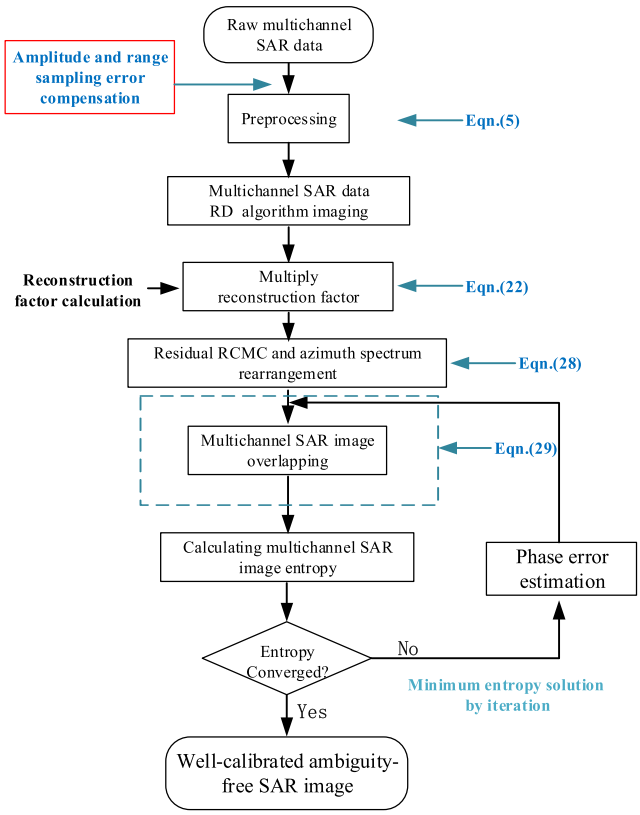

Fig. 3. Processing flowchart of the proposed method.

SAR radar records data in the 2-D time domain of fast time and slow time. For strip imaging, the route should be the azimuth axis, the vertical axis should be the distance axis, and the center line of the strip scene parallel to the route should be used as the reference line, whose distance is $R_b = \sqrt{h^2 + y^2}$. With the movement of the radar platform, the instantaneous slope distance equation from any scattering point in the scene to the *m*th channel is expressed as

$$R_m(t_a) = \sqrt{R_b^2 + (x - vt_a - d_m)^2}. \tag{1}$$

Then, the expression of the range time domain-azimuth time domain of the echo signal of the *m*th channel is as follows:

$$\begin{aligned} &s_m(t_r, t_a) \\ &= h(t_r) g(t_a - \frac{x + d_m}{v}) w(d_m) \\ &\exp\left(j\pi\gamma\left(t_r - \frac{2R_m(t_a)}{c}\right)^2\right) \exp\left(-j\frac{4\pi}{\lambda} R_m(t_a)\right) \end{aligned} \tag{2}$$

where γ denotes the chirp rate of the transmitted signal, c is the light speed, and λ denotes the wavelength of carrier signal. $h(t_r)$ and $g(t_a)$are the window functions in the range fast time and azimuth slow time, respectively, $w(d_m)$ is the weight of *m*th channel antenna.

Assuming that the azimuth ambiguity number is $N = 2I+1$ (I is a positive integer), then the 2-D spectral expression $S_m(f_r, f_a)$ of the range frequency domain-azimuth frequency domain of the echo signal of the *m*th channel is

$$\begin{aligned} S_m(f_r, f_a) &= \sum_{i=-I}^{I} \zeta_m \exp(j\Delta\vartheta_m) \exp(-j2\pi f_r \Delta\tau_m) \\ &\cdot S'_0(f_r, f_a + i \cdot f_p) \exp(j2\pi d_m (f_a + i \cdot f_p)/v) \end{aligned} \tag{3}$$

$$\begin{aligned} &S'_0(f_r, f_a + i \cdot f_p) \\ &= \iint \sigma(x, y) H(f_r) G(f_a + i \cdot f_p) \exp\left(-j\frac{2\pi R_b f_r^2}{\gamma}\right) \\ &\exp\left(-j\frac{2\pi(f_a + i \cdot f_p)x}{v}\right) \exp(j\Phi(f_r, f_a + i \cdot f_p; R_b)) dxdy \end{aligned} \tag{3a}$$

$$\begin{aligned} &\Phi(f_r, f_a + i \cdot f_p; R_b) \\ &= -4\pi R_b \sqrt{\left(\frac{f_r + f_c}{c}\right)^2 - \left(\frac{f_a + i \cdot f_p}{2v}\right)^2} \end{aligned} \tag{3b}$$

where f_r denotes range frequency and f_a azimuth frequency. *i* is the serial number of the ambiguous orientation, f_p denotes PRF, ζ_m is amplitude error of *m*th channel, $\Delta\vartheta_m$ is phase error of *m*th channel, and $\Delta\tau_m$ is range sampling time error of *m*th channel. $S'_0(f_r, f_a + i \cdot f_p)$ denotes the 2-D spectrum expression of reference channel with the *i*th ambiguity component. $H(f_r)$ and $G(f_a)$ the corresponding frequency domain expression of $h(t_r)$and $g(t_a)$, respectively. Carry out the second-order Taylor expansion of (3b) and omit the higher-order terms to get

$$\begin{aligned} &\Phi(f_r, f_a + i \cdot f_p; R_b) \approx \\ &\beta_0(f_a; i) + \beta_1(f_a; i) f_r + \beta_2(f_a; i) f_r^2 + o(f_2^2) \end{aligned} \tag{4}$$

$$\beta_0(f_a; i) = -\frac{2\pi R_b}{v} \sqrt{f_{aM}^2 - (f_a + i \cdot f_p)^2} \tag{4a}$$

$$\beta_1(f_a; i) = -\frac{4\pi R_b}{c} \left(1 + \frac{1}{2}(f_a + i \cdot f_p / f_{aM})^2\right) \tag{4b}$$

$$\beta_2(f_a; i) = \pi R_b \frac{2\lambda((f_a + i \cdot f_p)/f_{aM})^2}{c^2\left(1 - ((f_a + i \cdot f_p)/f_{aM})^2\right)^{3/2}}. \tag{4c}$$

In the following formula derivation, we will use (4) approximation instead of (3b). The amplitude error and range sampling time error can be handled by the method in [27]. Thus, these two types of error are not considered in the following derivation. In this article, we focus on the estimation of channel phase error.

The minimum entropy error estimation method proposed in this article evaluates the image entropy value of the SAR image imaged in the azimuth time domain. For subsequent processing in the azimuth time image domain, we first need to preprocess in the azimuth frequency domain, i.e., multiply by the following preprocessing function:

$$\mathrm{H}_1\left(f_a\right)=\exp\left(-j2\pi f_a\frac{d_m}{v}\right) \tag{5}$$

d_m/v represents the time delay in azimuth caused by the different receiving channel along fight route. $\mathrm{H}_1(f_a)$ is a linear phase in azimuth frequency domain, resulting a time delay d_m/v for the *m*th channel data in azimuth. After compensating $\mathrm{H}_1(f_a)$ for (3), the multichannel SAR data achieves "alignment" in the azimuth time domain. The advantages of preprocessing the data will be analyzed in later sections.

After formula (3) is compensated by formula (5), the following expression is obtained after formal simplification:

$$S_m\left(f_r,f_a\right)=\sum_{i=-I}^{I}\exp\left(j\Delta\vartheta_m\right)\cdot\phi_{i,m}S'_{0,i} \tag{6}$$

where

$$\phi_{i,m}=\exp\left(j2\pi\frac{d_m}{v}\left(i\cdot f_p\right)\right). \tag{6a}$$

To simplify the following expressions, we use notations $S'_{0,i}$ to substitute for $S'_0(f_r,f_a+i\cdot f_p)$, $\phi_{i,m}$ is the phase term to construct multichannel steering vector.

We can find that after the preprocessing of (5), the phase term of the steering vector of the multichannel SAR data is not related to the azimuth frequency domain, but only related to the channel and azimuth ambiguity. Then, if the multichannel SAR data is transformed into the azimuth time domain, the steering vector of the entire azimuth time domain will be a constant vector related to the number of channels and ambiguous numbers, which will greatly simplify the construction of the azimuth time domain steering vector and facilitate subsequent key operations such as image reconstruction are performed in the image domain of the azimuth time domain.

III. Processing Method

A. Multichannel SAR Imaging and Reconstruction

In the method proposed in this article, the imaging processing operation of multichannel SAR data adopts the range Doppler (RD) algorithm of frequency domain RCM.

Since the data of each channel is undersampled in the azimuth direction, i.e., there is azimuth ambiguity, the RCMs of the ambiguous components of different ambiguous numbers are different, and these ambiguous components overlap in the azimuth frequency domain, so in this section the imaging processing is to correct RCM of the baseband frequency (i.e., the case of $i=0$), and its RCM correction and range compression function can be expressed as

$$H_{\mathrm{rmc}}\left(f_a,f_r\right)=\exp\left(j\frac{4\pi R_b}{c}\left(1+\frac{1}{2}\left(f_a/f_{aM}\right)^2\right)f_r\right) \tag{7}$$

$$H_2\left(f_a,f_r\right)=\exp\left(j\pi R_b f_r^2 K\left(f_a\right)\right) \tag{7a}$$

where $K=1/\gamma-\beta_2$.

After (6) is compensated for baseband RCM correction (RCMC) by (7) and range compression by (7a), the 2-D frequency domain expression is as follows:

$$S_{c,m}\left(f_r,f_a\right)=\sum_{i=-I}^{I}\exp\left(j\Delta\vartheta_m\right)\phi_{i,m}S'_{1,i} \tag{8}$$

where

$$\begin{aligned}S'_{1,i}&=S'_{0,i}\cdot H_{\mathrm{rmc}}\left(f_a,f_r\right)H_2\left(f_a,f_r\right)\\&=\int\int\sigma\left(x,y\right)H\left(f_r\right)G_i\cdot\exp\left(-j2\pi\left(f_a+i\cdot f_p\right)\frac{x}{v}\right)\\&\exp\left(-j\frac{2\pi R_b}{v}\sqrt{f_{aM}^2-\left(f_a+i\cdot f_p\right)^2}\right)\\&\exp\left(-j\left(4\pi R_b\frac{2\left(i\cdot f_p\right)f_a+\left(i\cdot f_p\right)^2}{2cf_{aM}^2}\right)f_r\right)\\&\exp\left(j\left(\beta_2\left(f_a\right)-\beta_2\left(f_a+i\cdot f_p\right)\right)f_r^2\right)dxdy.\end{aligned} \tag{9}$$

The next operation is to perform azimuth matched filtering. The azimuth matched filter function can be expressed as

$$H_{ref}=\exp\left(j\frac{2\pi R_b}{v}\sqrt{f_{aM}^2-f_a^2}\right). \tag{10}$$

Multiply (8) by (10), and then perform the inverse Fourier transform of the azimuth to transform it into the azimuth time domain. After azimuth matched filtering, the expression of the signal of the *m*th channel is transformed into the 2-D time domain, and the expression of the 2-D time domain $\mathbf{F}_{c,m}(t_r,t_a)$ is

$$\begin{aligned}&\mathbf{F}_{c,m}\left(t_r,t_a\right)\\&=\sum_{i=-I}^{I}\exp\left(j\Delta\vartheta_m\right)\cdot\exp\left(j2\pi i\cdot f_p\frac{d_m}{v}\right)\cdot\\&F_i'\left(t_r,t_a\right)\end{aligned} \tag{11}$$

$$F_i'\left(t_r,t_a\right)=IFT2\left\{S'_{2,i}\right\} \tag{12}$$

$$\begin{aligned}S'_{2,i}&=S'_{1,i}\cdot H_{ref}\\&=\int\int\sigma\left(x,y\right)H\left(f_r\right)G_i\cdot\phi_{mct,i}\\&\exp\left(-j2\pi\left(f_a+i\cdot f_p\right)\frac{x}{v}\right)\\&\exp\left(-j4\pi R_b\cdot\frac{2\left(i\cdot f_p\right)f_a+\left(i\cdot f_p\right)^2}{2cf_{aM}^2}\cdot f_r\right)\\&\exp\left(j\left(\beta_2\left(f_a\right)-\beta_2\left(f_a+i\cdot f_p\right)\right)f_r^2\right)dxdy\end{aligned} \tag{13}$$

where $F_i'(t_r,t_a)$ denotes the imaging results of the *i*th Doppler ambiguity component by using RD algorithm. IFT2 represents the operator of 2-D inverse Fourier transform.

In order to facilitate further formula derivation, the images of all M channels are written as the following image set:

$$\mathbf{F}_c = \left[\begin{array}{cccccc} \mathbf{F}_{c,1} & \cdots & \mathbf{F}_{c,m} & \cdots & \mathbf{F}_{c,M} \end{array} \right]^{\mathrm{T}}. \tag{14}$$

For the sake of brevity, the multichannel image set $\mathbf{F}_c$ can be matrixed as

$$\mathbf{F}_c = \Gamma \mathbf{A} \mathbf{F}'(t_r,t_a) \tag{15}$$

$$\Gamma = diag \left[\begin{array}{ccccc} \exp(j\vartheta_1) & \cdots & \exp(j\vartheta_m) & \cdots & \exp(j\vartheta_M) \end{array} \right] \tag{16}$$

$$\mathbf{F}'(t_r,t_a) = \left[\begin{array}{cccc} F'_{-I} & \cdots & F'_i & \cdots & F'_I \end{array} \right]^{\mathrm{T}} \tag{17}$$

$$\mathbf{A} = \left[\begin{array}{cccc} \mathbf{a}_{-I} & \cdots & \mathbf{a}_i & \cdots & \mathbf{a}_I \end{array} \right] \tag{18}$$

$$\mathbf{a}_i = \left[\begin{array}{cccc} \kappa_{1,i} & \cdots & \kappa_{m,i} & \cdots & \kappa_{M,i} \end{array} \right]^{\mathrm{T}} \tag{19}$$

$$\kappa_{m,i} = \exp\left(j2\pi \left(i \cdot f_p \right) \frac{d_m}{v} \right) \tag{20}$$

where Γ represents a diagonal matrix of channel phase error terms, $diag[\mathbf{x}]$ represents the operator that rewrites the vector $\mathbf{x}$ into a diagonal matrix with the vector $\mathbf{x}$ as the diagonal elements. $\exp(j\Delta\vartheta_m)$ is phase error term of *m*th channel relative to the reference channel. If channel 1 is the reference channel $\Delta\vartheta_1$ is 0. $\mathbf{F}'(t_r,t_a)$ consists of $(2I+1)$ imaging results of ambiguity component. Matrix $\mathbf{A}$ is the steering vector matrix for multichannel SAR in the image domain, and due to the preprocessing in the previous section. The steering vector matrix in the multichannel image domain is a constant related to the number of channels and the number of ambiguities for the entire image.

Then, the system function method in [20] is used to reconstruct a high-resolution wide image without ambiguity by inverting the system function (i.e., the steering vector matrix). A matrix inversion can be done. The inverse filter matrix for image reconstruction can be obtained by the following formula and can be written in the form of $(2I+1)$ row vectors:

$$\mathbf{P} = \mathbf{A}^{-1} = \left[\begin{array}{cccccc} \mathbf{p}_{-I}^{\mathrm{T}} & \cdots & \mathbf{p}_i^{\mathrm{T}} & \cdots & \mathbf{p}_I^{\mathrm{T}} \end{array} \right]^{\mathrm{T}} \tag{21}$$

where the size of vector $\mathbf{p}_i$ is $1 \times \mathrm{M}$. $\mathbf{p}_i$ is the reconstruction factor vector to extract the image of the *i*th ambiguity. Multiply vector $\mathbf{p}_i$ for multichannel SAR images set $\mathbf{F}_c$, the image of the *i*th ambiguity component can be achieved

$$\begin{aligned} \mathbf{I}_i(t_r,t_a) &= \mathbf{p}_i \mathbf{F}_{\mathrm{c}} \\ &= \mathbf{p}_i \Gamma \mathbf{A} \mathbf{F}'. \end{aligned} \tag{22}$$

However, it is noticed that the SAR image represented by $\mathbf{I}_i(t_r,t_a)$ has residual RCM in case of $i \neq 0$. Thus, $\mathbf{I}_i(t_r,t_a)$ is not fine-focused unless the residual RCM is corrected [12]. Except for residual RCM correction (rRCMC), a time shift operation is required to construct a full Doppler spectrum. The compensation function of rRCMC and time shift operation can be expressed as

$$H_{\mathrm{rem},i}(f_r,f_a) = \exp\left(j4\pi R_b \cdot \frac{2\left(i \cdot f_p\right) f_a + \left(i \cdot f_p\right)^2}{2cf_{aM}^2} \cdot f_r \right) \tag{23}$$

$$H_{tf,i}(f_r,f_a) = \exp\left(-j2\pi f_a \frac{\left(i \cdot f_p\right) v^2}{\lambda R_b} \right). \tag{24}$$

If a higher requirement for imaging resolution, a rSRC needs to be considered. The compensation function of rSRC can be expressed as

$$H_{\mathrm{rsrc},i}(f_r,f_a) = \exp\left(-j\left(\beta_2(f_a) - \beta_2\left(f_a + i \cdot f_p\right) \right) f_r^2 \right). \tag{25}$$

Equations (23)–(25) can be compensated in 2-D frequency domain by

$$H_3(f_a,f_r;i) = H_{tf,i} \cdot H_{\mathrm{rem},i} \cdot H_{\mathrm{rsrc},i}. \tag{26}$$

The corresponding 2-D spectrum of the coarse focused image $\mathbf{I}_i(\tau,t_a)$, i.e., $\mathbf{S}_{f,i}(f_r,f_a)$ can be expressed as

$$\mathbf{S}_{f,i}(f_r,f_a) = \mathrm{FT2}\left[\mathbf{I}_i(t_r,t_a)\right] \tag{27}$$

where FT2 represents the operator of 2-D Fourier transform. Then, we construct the ambiguous Doppler spectrum of the *m*th channel

The reconstructed full-spectrum signal (28) is subjected to 2-D Fourier transform,and the final ambiguity-free HRWS SAR image can be obtained as is shown in Fig.2 which is expressed as follows: (28) shown at the bottom of this page,

$$\mathbf{I}(t_r,t_a) = \sum_{m=1}^{M} \exp(-j\Delta\theta_m) \cdot \mathbf{I}_m^{\mathrm{full}}(t_r,t_a) \tag{29}$$

where

$$\mathbf{I}_m^{\mathrm{full}}(t_r,t_a) = \mathrm{IFFT2}\left[\mathbf{I}_{f,m}^{\mathrm{full}}(f_r,f_a)\right]. \tag{30}$$

B. Fine-Focused SAR Image Entropy and Error Estimation Flow

$\mathbf{I}(n,k)$ and $\mathbf{I}_m^{\mathrm{full}}(n,k)$ are the discrete expression of, respectively, image$\mathbf{I}(t_r,t_a)$ and image $\mathbf{I}_m^{\mathrm{full}}(t_r,t_a)$

$$I(n,k) = \sum_{m=1}^{M} \exp(-j\Delta\theta_m) \cdot I_m^{\mathrm{full}}(n,k). \tag{31}$$

Calculate the fine-focused image entropy of $I(n,k)$

$$\varepsilon\left\{ \left| I(n,k) \right|^2 \right\} = \sum_{n=0}^{N-1} \sum_{k=0}^{K-1} \frac{\left| I(n,k) \right|^2}{E_S} \ln \frac{E_S}{\left| I(n,k) \right|^2} \tag{32}$$

where

$$E_S = \sum_{n=0}^{N-1} \sum_{k=0}^{K-1} \left| I(n,k) \right|^2. \tag{33}$$

$$\mathbf{I}_m^{\mathrm{full}}(f_r,f_a) = \left[\mathbf{S}_{f,-I,m} H_3(f_a,f_r;-I) \ \cdots \ \mathbf{S}_{f,i,m} H_3(f_a,f_r;-i) \ \cdots \ \mathbf{S}_{f,I,m} H_3(f_a,f_r;I) \right] \tag{28}$$

Equation (32) can be converted as

$$\varepsilon\left\{|I(n,k)|^2\right\} = -\frac{1}{E_S}\sum_{n=0}^{N-1}\sum_{k=0}^{K-1}|I(n,k)|^2\ln|I(n,k)|^2 + \ln E_S. \tag{34}$$

The fine-focused image entropy in (34) is considered as the objective function, the channel phase error $\mathbf{w} = [\ \exp(j\vartheta_1)\ \cdots\ \exp(j\vartheta_m)\ \cdots\ \exp(j\vartheta_M)\ ]$ is a variable to be solved. The channel error estimation can be formulated as an optimization

$$\mathbf{w} = \arg\min_{\mathbf{w}}\left(\varepsilon\left\{|I(n,k)|^2\right\}\right). \tag{35}$$

Equation (35) has no closed solution and an iteration process is needed. In [29], referencing the monotonic iterative method in [33] and [34], a minimum entropy for multichannel SAR phase error estimation is presented. A Polynomial-fit-based minimum entropy adapted for multichannel SAR phase error estimation is proposed in [35], which can speed up the solution process. In addition, (35) can also be handled by BFGS algorithm in. For a better comparison with the ME in [36], we chose the same solution approach as.

In practice, if amplitude error and range sampling time error are needed to be considered, compensation can be performed for the raw multichannel data before preprocessing by the calibration method. The processing flow of the minimum entropy channel phase error estimation based on RD imaging proposed in this article is shown in Fig.3 and can be described as follows.

Step 1: The raw data is preprocessed to compensate the linear phase in Doppler, so that the multichannel SAR data can be "aligned" in the azimuth time domain.

Step 2: The preprocessed multichannel SAR data of each channel is independently imaged, and the imaging algorithm adopts the range Doppler algorithm to correct the range walk in the frequency domain, and then the SAR images with azimuth ambiguity of multiple channels are obtained.

Step 3: Multiply the constructed reconstruction factor by the SAR image for each channel separately.

Step 4: The SAR images with corresponding reconstructed factors are subjected to residual RCM compensation and azimuth spectral rearrangement.

Step 5: After Step 4, a multichannel SAR image is obtained for calculating the entropy of the finely focused image and obtaining the final ambiguity-free SAR image. After adding the multichannel SAR images, we obtain the reconstructed SAR image.

Step 6: Calculate the entropy value of the SAR image obtained in Step 5, obtain the entropy value of the SAR image, and determine whether the entropy value converges.

Step 7: Perform multichannel minimum entropy channel error estimation, and compensate the channel error to the multichannel SAR image obtained after Step 4, and continue to perform the steps after Step 4 in sequence until the entropy value converges to obtain the error-compensated ambiguity-free image. High-resolution wide-format SAR image.

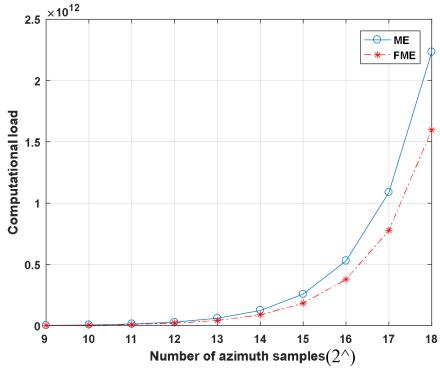

Fig. 4. Comparison of the computational complexity between the ME and the FME in the case of $M = 5$ and $N = 3$.

IV. Computational Complexity Analysis

In order to quantitatively analyze the improvement in computational efficiency of the method proposed in this article, the computational complexity in the processing of the two methods is evaluated. Disregarding the difference in the calculation amount of the two methods in the error iterative estimation part and the reconstruction factor calculation part, only the calculation amount of the multichannel imaging and reconstruction part is calculated. Since complex multiplication often consumes more computing resources in the calculation, only the number of complex multiplications is considered in the calculation amount analysis. The number of channels, the number of azimuth ambiguities, the number of distance sampling points, and the number of azimuth sampling points of the current channel data are represented by *M*, *N*, *Y*r, and *Y*a, respectively.

In the literature [29], after using coarsely focused SAR imaging for error estimation, the estimated error needs to be compensated into the original multichannel data, and the final error-corrected SAR image can be obtained after additional reconstruction and imaging. In the additional imaging of the traditional ME method, the same RD algorithm as in this article was used for imaging.

The overall computational complexity of the minimum entropy method in [29] is

$$\mathrm{C_{ME}} = \frac{Y_a Y_r}{2}((2M+MN+N)\log_2 Y_r + (MN+4N)\log_2 Y_a + (MN+2N)\log_2 N + 6MN+4M+6N). \tag{36}$$

The overall computational complexity of the minimum entropy method based on RD in this article is

$$\mathrm{C_{FME}} = \frac{MY_aY_r}{2}\left((1+N)\log_2 Y_r Y_a + N\log_2 N + 4N + 4\right). \tag{37}$$

Fig. 4 shows the comparison of the computational complexity between the ME and the FME in the case of $M = 5$ and $N = 3$. The proposed method (mentioned as FME in Fig. 4) has a smaller computational load. For a better demonstration of computational load improvement by the proposed method compared with traditional ME, we define a computational load

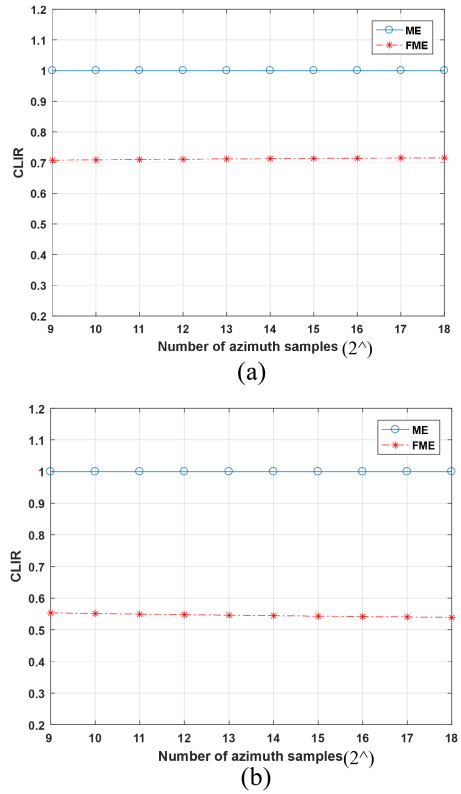

Fig. 5. CILR in the case of (a) $M = 5$ and $N = 3$; (b) $M = 2$ and $N = 2$.

improvement ratio (CLIR)

$$\mathrm{CLIR} = \frac{\mathrm{C_{FME}}}{\mathrm{C_{ME}}}. \tag{38}$$

From (37), we know that a CLIR less than 1 means that the proposed method has an improvement on computational complexity. Specially, the CLIR of the traditional ME is equal to 1.

Fig. 5 shows CILR calculated by (35)–(37) in two kinds of multichannel SAR systems with different channel number and ambiguity number. In the case of $M = 5$ and $N = 3$, the CLIR of FME method is 0.7, and increases slightly with the increase of azimuth sample number. It means that the proposed FME method brings a reduction of computational load by 30% approximately. In the first case in Fig. 5(a), channel number is greater than ambiguity number. However, in the area of space-borne multichannel SAR, channel number usually do not exceed to ambiguity. For example, Radarsat-2 and Gaofen-3 are both dual-channel SAR systems whose ambiguity numbers are about 2. Thus, the case of $M = N$ is worthy to be investigated. Fig. 5(b) shows the CLIR in the case of $M = 2$ and $N = 2$. We can find that the proposed FME method brings a reduction of computational load by 45% approximately. Computational complexity analysis demonstrates that the proposed method is an efficient approach to realizing HRWS SAR imaging with the channel phase error calibrated.

It is worth noting that for the two parts of the calculation that are not considered in signal processing. Two methods have little difference in the number of iterations for error iterative estimation, which will be validated in the subsequent simulation experiments. However, in the proposed method, the entire scene method shares a constant reconstruction factor, which does not vary with the azimuth frequency due to the preprocessing. Since the reconstruction factor only need to be calculated for once during the reconstruction factor calculation and generation, which will further expand the advantage in computational complexity of the proposed method

TABLE I
SIMULATION PARAMETERS

Parameters	Value
Carrier frequency	0.0555 m
Bandwidth	100 MHz
Velocity	180 m/s
Rs	15 km
PRF	240 Hz
Pulse width	16e-6s
Channel Number	5
Azimuth ambiguity number	3
Da	3 m

V. RESULTS

In this section, simulated data and acquired space-borne and airborne data are processed to validate the proposed method.

A. Simulated Data Experiment

In the simulation experiments in this section, the echo data is obtained by point simulation of the airborne 5-channel SAR system. The system parameters of the simulation experiment are shown in the Table I the platform speed is 180 m/s, PRF = 240 Hz, the slant distance from the scene center to the radar platform is 15 km, the transmitted signal is C-band, and the bandwidth is 100 MHz. The five antenna channels are distributed along the direction of radar movement. The channel located in the center transmits the chirp signal, and all channels receive the echo as the receive channel. The Doppler bandwidth of the echo calculated according to the size of the transmitting antenna is approximately 600 Hz, and the ambiguity number is approximately 3 because the PRF is 240 Hz.

In this simulation experiment, the original error of the channel is set as a constant phase error, as shown in Table II. The channel phase error is added to the echo for each channel in the echo simulation. In this section, the results of the multichannel minimum entropy channel error estimation method based on RD imaging proposed in this article and the results of the classical multichannel minimum entropy error estimation method are compared to verify the effectiveness of the method proposed.

Fig. 6 is the original data obtained by point simulation in this section, taking the channel 1 data as an example, in which Fig. 6(a) is the echo in the 2-D time domain of channel 1, and Fig. 6(b) is the 2-D frequency domain echo. It can be seen that since the multichannel SAR is under-sampled in azimuth, the

TABLE II
CHANNEL PHASE ERROR ESTIMATION RESULTS WITH SNR=20 DB

	Phase Error (degree)	Channel 1	Channel 2	Channel 3	Channel 4	Channel 5
	Initial Error	-25	40	0	-15	-65
The Proposed	Estimated value	-24.907	40.039	0	-14.954	-64.920
	Deviation	-0.093	0.039	0	-0.045	-0.080
ME	Estimated value	-24.926	40.018	0	-14.943	-64.912
	Deviation	-0.074	0.018	0	-0.057	-0.088

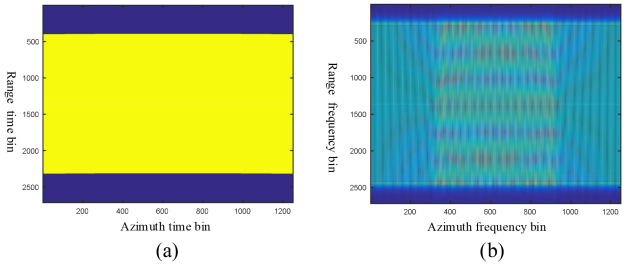

Fig. 6. Raw simulated data of channel 1 in (a) two-dimensional time domain and (b) two-dimensional frequency domain.

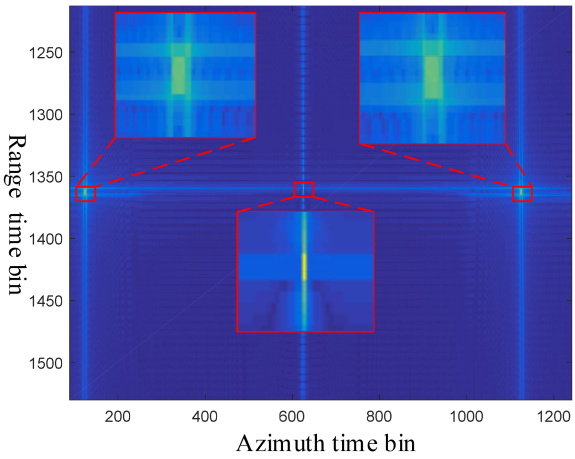

Fig. 7. SAR image of channel 1 after RD imaging.

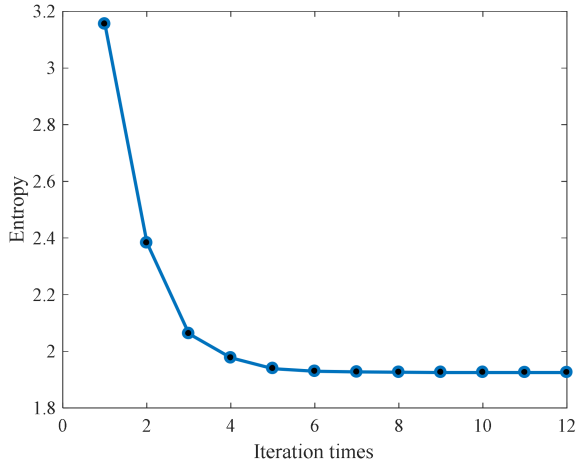

Fig. 8. Curve of the entropy value of the proposed method with the number of iterations.

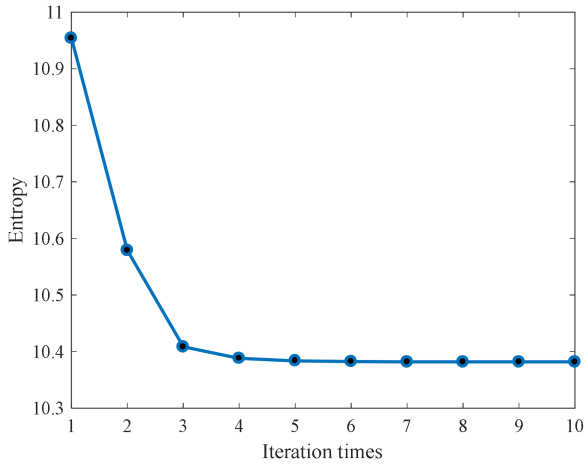

Fig. 9. Curve of the entropy value of the traditional minimum entropy method with the number of iterations.

spectrum of a single channel echo in the azimuth frequency domain is folded.

Fig. 7 is the result of RD imaging for multichannel SAR. It can be seen that a single point target forms an ambiguous point in the azimuth time domain due to azimuth undersampling.

As shown in Table II, when the signal-to-noise ratio SNR is 20 dB, the original minimum entropy error estimation algorithm and the traditional classic minimum entropy error estimation results are compared under the condition of five channels and three ambiguities. The second row in the table is added to channel phase error in simulated multichannel SAR data. The third row is the channel error estimated by the minimum entropy method based on RD imaging proposed in this article. It can be found that the method proposed in this article is effective for channel phase error estimation. The fifth row is the channel phase error estimated by the classical minimum entropy channel error estimation method. In addition, the estimated biases for both methods are given in the table. Figs. 8 and 9 show the entropy change curve and the channel error estimation results of the method proposed in this article and the traditional minimum

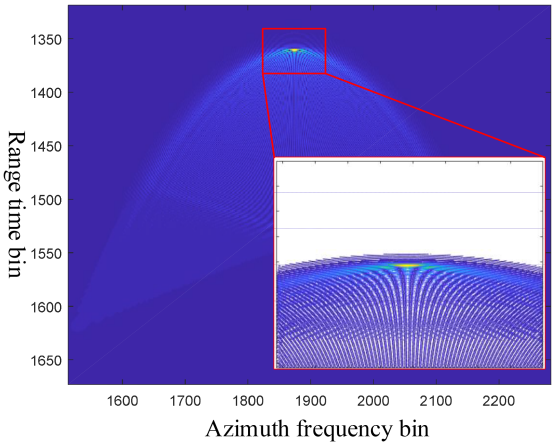

Fig. 10. SAR image after performing the phase error estimation by traditional ME.

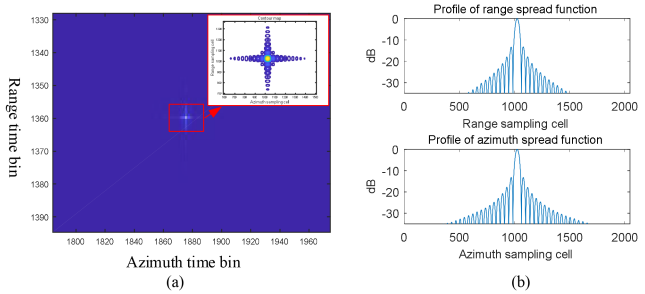

Fig. 11. SAR image after performing the phase error estimation by the proposed method. (a) Point target imaging result. (b) Range and azimuth profile of the point target.

entropy method in the channel error estimation process, respectively. Combining the estimation results listed in Table II and the curves shown in Figs. 8 and 9, it can be seen that the method proposed in this article has the same channel error estimation accuracy as the classical minimum entropy method.

Under the condition that the signal-to-noise ratio is 20 dB, the SAR images obtained directly after the error estimation of the method proposed in this article and the traditional minimum entropy method are given.

Fig. 10 is a SAR image obtained directly after the error estimation by traditional minimum entropy is completed, and the image here is the SAR image used to calculate the image entropy value in the process of estimating the error. It can be seen from Fig. 10 that the image is coarsely focused, which is azimuthal imaging directly through the azimuth deramp, without correcting for range migration. Therefore, this coarsely focused image cannot be used for the final SAR image.

Therefore, the estimated channel error here can only be used to compensate for the multichannel SAR data, and then perform additional multichannel SAR reconstruction and imaging processing.

Fig. 11 is the SAR image directly obtained by the minimum entropy method proposed in this article after the error estimation. It can be seen from Fig. 11(a) and (b) that the point target is fully focused in two dimensions. And, since the reconstruction and channel errors have been compensated, the ambiguity in the azimuth direction is also well suppressed.

TABLE III
PARAMETERS OF GAOFEN-3 DUAL-CHANNEL SAR

Parameters	Value
Wavelength	0.0555 m
Bandwidth	80 MHz
Velocity	7100 m/s
Rs	1080 km
PRF	1981.4 Hz
Pulse width	54e-6s
Channel number	2
Azimuth ambiguity number	2
Antenna azimuth aperture length	7.5 m

B. Space-Borne Acquired SAR Data Processing

In the simulation experiments in this section, the echo data is the dual-channel strip data recorded by Gaofen-3 SAR satellite. The system parameters in this mode are shown in the Table III: the platform speed is 7100 m/s, PRF = 1981.4 Hz, the slant distance from the scene center to the radar platform is 1080 km, the transmitted signal is C-band, and the bandwidth is 80 MHz. The Gaofen-3 SAR satellite has two azimuth antenna channels distributed along the direction of radar movement. One channel transmits a chirp signal, and the two channels are both receiving channels to receive echoes. The ambiguity number of the azimuth Doppler bandwidth calculated according to the size of the transmitting antenna is approximately 2.

For the dual-channel data recorded by the Gaofen-3 SAR satellite in this mode, it can be seen that the number of channels in this system is less, and the azimuth ambiguity number is equal to the azimuth channel. Therefore, in this mode, the system does not have redundant space freedom, and in this case, the channel error estimation method of the subspace class cannot be applied to the estimation of the channel error in this case. Therefore, in this case, image-based measures (such as the minimum entropy method based on RD imaging fine-focus images proposed in this section) are applicable.

Fig. 12 shows the image entropy value change curve of the minimum entropy estimation method based on fine focusing proposed in this article in the process of channel error estimation. It can be seen that the image entropy value is close to convergence after three iterations. Fig. 10 shows the estimated two-channel SAR channel phase error. Fig. 13 shows the interference phase of the two-channel data in the 2-D frequency domain obtained by compensating the phase error shown in Fig. 14 for the two-channel data.

Fig. 15 is the imaging results after reconstruction by RD algorithm without channel phase error compensation. We can see that azimuth ghosts appear along the azimuth direction of the SAR image as the results of channel phase error. The image is obtained by the azimuth deramp operation to obtain a frequency domain image. Since the distance migration has not been corrected, the image is coarsely focused. Therefore,

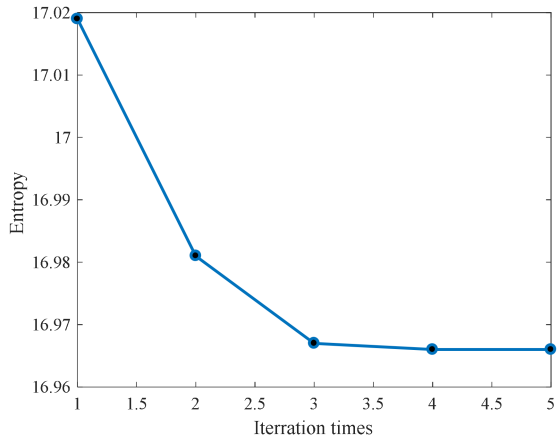

Fig. 12. Curve of the entropy value of the proposed method with the number of iterations.

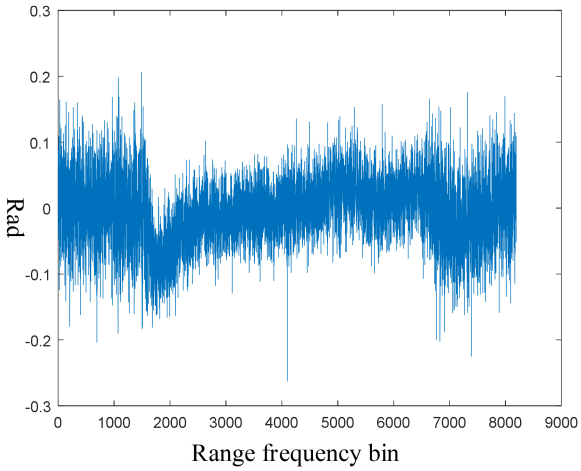

Fig. 13. Interference phase between two channel after the estimated channel phase error compensated.

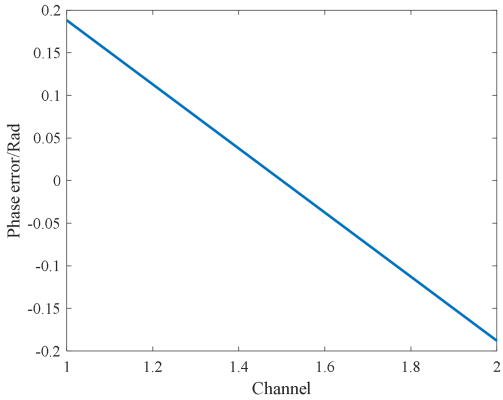

Fig. 14. Channel phase error estimation results by the proposed method.

using the azimuth deramp-based coarsely focused image in the channel error estimation process can only be applied to the phase error estimation. The result shown in Fig. 16 is the result obtained by the minimum entropy method based on RD imaging proposed in this article after channel error estimation. It can be seen from the figure that the azimuth ambiguity caused by

Fig. 15. Imaging results after reconstruction by RD algorithm without channel phase error compensation.

Fig. 16. Fine-focused SAR image by the proposed method after channel error estimation.

TABLE IV
PARAMETERS OF AIR-BORNE SEVEN-CHANNEL SAR

Parameters	Value
Wavelength	0.054 m
Bandwidth	150 MHz
Velocity	108/s
Rs	12 km
PRF	200 Hz
Pulse width	20e-6s
Channel Number	7
Azimuth ambiguity number	5
Antenna azimuth Aperture length	1.7 m

channel error compensation channel error has been effectively suppressed compared with Fig. 15, and the imaging the result is finely focused.

C. Air-Borne Acquired SAR Data Processing

The air-borne multichannel SAR data is collected by an azimuth 7-channel SAR system. The system parameters in this mode are shown in the Table IV: the platform speed is 108 m/s, PRF = 1981.4 Hz, the slant distance from the scene center to the radar platform is 1080 km, the transmitted signal is C-band, and the bandwidth is 80 MHz. One channel transmits a chirp signal, and the 7 channels are both receiving channels to receive echoes. The ambiguity number of the azimuth Doppler bandwidth calculated according to the size of the transmitting antenna is approximately 5.

TABLE V
CHANNEL PHASE ERROR ESTIMATION RESULTS WITH SNR=20 DB

(degree)	Ch1	Ch2	Ch3	Ch4	Chl5	Ch6	Ch7	Entropy value
SSP	20.609	11.124	9.945	0	-16.377	-29.392	-33.344	8.0764e4
ME	41.195	25.781	15.357	0.576	-12.755	-27.324	-42.830	5.4228e4
The Proposed	45.832	31.531	15.673	0.561	-12.571	-32.369	-48.657	5.3672e4

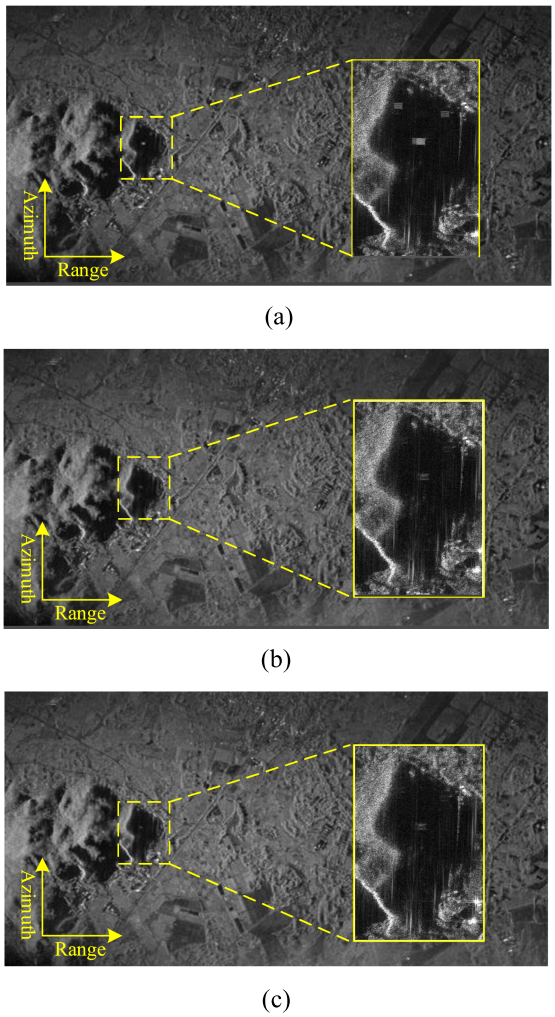

Fig. 17. Imaging results of different methods and their local enlargements. (a) SSP method. (b) Traditional ME method based on azimuth deramp. (c) Proposed FME method.

In this section, we make a comparison between the SSP method in [27], the traditional ME method and the proposed method. For a better comparison, in the imaging processing after using the SSP method and the traditional ME method, we use the same imaging algorithm with the proposed FME method.

Fig. 17 shows the second acquired data processing results by the three different methods. Fig. 17(a) is the SAR image after compensated by the SSP method. Fig. 17(b) is the SAR image obtained by the traditional ME method. Fig. 17(c) is the SAR image obtained by the proposed FME method. We can see from the enlargements of three figures that the SSP method produces a bad ghost suppression result compared with the other two methods, i.e., the traditional ME and the proposed FME method. For a fine-focused SAR image, the traditional one requires another reconstruction and imaging processing. Fig. 17(b) and (c) shows that two methods achieve the nearly same suppression effect for the azimuth ghost.

Table V shows the channel phase error estimation results by three methods with SNR equals 20 dB. The estimated values are listed and the last column shows the image entropy of the imaging results by three methods. We can see that the proposed FME method achieves a smallest entropy value, which means that the proposed method has a more accurate estimation for channel phase error.

VI. SUMMARY AND DISCUSSION

According to the experimental evaluation in processing of simulated data and acquired data, the proposed FME method achieves as good performance as the traditional ME method in channel phase error estimation. However, for a well-calibrated HRWS SAR image, the proposed method brings a considerable reduction in computational complexity evidently. The underlying principles can be explained from two aspects. On the one hand, thanks to the preprocessing, the entire SAR data share the constant reconstruction factor, which are independent with azimuth frequency. It means that the proposed method requires less computation when determine the reconstruction factor. On the other hand, the proposed method performs channel error estimation by using the fine-focused SAR images and the well-calibrated HRWS SAR image can be obtained directly after estimation, avoiding a redundant reconstruction and SAR imaging processing.

Future works includes extending this method to space-borne applications combined with unified focusing algorithm, which is adapted for more imaging mode and higher resolution.

This article proposes a minimum entropy channel error estimation method based on fine-focused image entropy. In the estimation process of the proposed method, each channel SAR image used has undergone the imaging of the RD algorithm and the residual RCM compensation. Therefore, the SAR image used in the channel error estimation process in this article can directly obtain the final fine focus after minimum entropy iterative compensation. Compared with the traditional minimum entropy method based on azimuth deramp, redundant reconstruction, and

imaging operations are reduced. Error estimation and imaging processing procedures are optimized and processing efficiency is improved evidently by a considerable range. Simulation experiments and acquired data processing verify the effectiveness of the method proposed in this article.

REFERENCES

[1] G. C. Sun, Y. Liu, J. Xiang, W. Liu, M. Xing, and J. Chen, "Spaceborne synthetic aperture radar imaging algorithms: An overview," *IEEE Geosci. Remote Sens. Mag.*, vol. 10, no. 1, pp. 161–184, Mar. 2022.

[2] A. Currie and M. A. Brown, "Wide-swath SAR," *IEE Proc. F - Radar Signal Process.*, vol. 139, no. 2, pp. 122–135, Apr. 1992.

[3] J. Chen, M. Xing, H. Yu, B. Liang, J. Peng, and G. C. Sun, "Motion compensation/autofocus in airborne synthetic aperture radar: A review," *IEEE Geosci. Remote Sens. Mag.*, vol. 10, no. 1, pp. 185–206, Mar. 2022.

[4] G. D. Callaghan and I. D. Longstaff, "Wide-swath space-borne SAR using a quad-element array," *IEE Proc. - Radar, Sonar Navigation*, vol. 146, no. 3, pp. 159–165, 1999.

[5] G. Farquharson, P. Lopez-Dekker, and S. J. Frasier, "Contrast-based phase calibration for remote sensing systems with digital beamforming antennas," *IEEE Trans. Geosci. Remote Sens.*, vol. 51, no. 3, pp. 1744–1754, Mar. 2013.

[6] Z. Li, H. Wang, T. Su, and Z. Bao, "Generation of wide-swath and high-resolution SAR images from multichannel small spaceborne SAR systems," *IEEE Geosci. Remote Sens. Lett.*, vol. 2, no. 1, pp. 82–86, Jan. 2005.

[7] N. Gebert, G. Krieger, and A. Moreira, "Multichannel azimuth processing in ScanSAR and TOPS mode operation," *IEEE Trans. Geosci. Remote Sens.*, vol. 48, no. 7, pp. 2994–3008, Jul. 2010.

[8] D. Bliss and K. Forsythe, "Multiple-input multiple-output (MIMO) radar and imaging: Degrees of freedom and resolution," in *Proc. 37th Asilomar Conf. Signals, Syst. Comput.*, 2003, pp. 54–59.

[9] P. Laskowski, F. Bordoni, and M. Younis, "Multi-channel SAR performance analysis in the presence of antenna excitation errors," in *Proc. 14th Int. Radar Symp.*, 2013, pp. 491–496.

[10] A. Luscombe, "Image quality and calibration of RADARSAT-2," pp. II–757–II–760.

[11] G. Krieger et al., "Advanced concepts for high-resolution wide-swath SAR imaging," pp. 1–4.

[12] J. Xiang et al., "A robust image-domain subspace-based channel error calibration and postimaging reconstruction algorithm for multiple azimuth channels SAR," *IEEE Trans. Geosci. Remote Sens.*, vol. 60, 2022, Art. no. 5215818.

[13] N. Gebert, G. Krieger, and A. Moreira, "Digital beamforming for HRWS-SAR imaging: System design, performance and optimization strategies," in *Proc. IEEE Int. Symp. Geosci. Remote Sens.*, 2006, pp. 1836–1839.

[14] M. Younis, C. Fischer, and W. Wiesbeck, "Digital beamforming in SAR systems," *IEEE Trans. Geosci. Remote Sens.*, vol. 41, no. 7, pp. 1735–1739, Jul. 2003.

[15] S.-S. Zuo, M. Xing, X.-G. Xia, and G.-C. Sun, "Improved signal reconstruction algorithm for multichannel SAR based on the doppler spectrum estimation," *IEEE J. Sel. Topics Appl. Earth Observ. Remote Sens.*, vol. 10, no. 4, pp. 1425–1442, Apr. 2017.

[16] L. Zhang, M.-D. Xing, C.-W. Qiu, and Z. Bao, "Adaptive two-step calibration for high-resolution and wide-swath SAR imaging," *IET Radar, Sonar Navigation*, vol. 4, no. 4, pp. 548–559, 2010.

[17] G. Sun, M. Xing, X. Xia, Y. Wu, and Z. Bao, "Multichannel full-aperture azimuth processing for beam steering SAR," in *Proc. Conf. Asia-Pacific Conf. Synthetic Aperture Radar*, 2013, pp. 206–209.

[18] Z. Li, S. Li, Z. Liu, H. Yang, J. Wu, and J. Yang., "Bistatic forward-looking SAR MP-DPCA method for space–time extension clutter suppression," *IEEE Trans. Geosci. Remote Sens.*, vol. 58, no. 9, pp. 6565–6579, Sep. 2020.

[19] W. Jing, M. Xing, C.-W. Qiu, Z. Bao, and T.-S. Yeo, "Unambiguous reconstruction and high-resolution imaging for multiple-channel SAR and airborne experiment results," *IEEE Geosci. Remote Sens. Lett.*, vol. 6, no. 1, pp. 102–106, Jan. 2009.

[20] G. Krieger, N. Gebert, and A. Moreira, "Unambiguous SAR signal reconstruction from nonuniform displaced phase center sampling," *IEEE Geosci. Remote Sens. Lett.*, vol. 1, no. 4, pp. 260–264, Oct. 2004.

[21] X. Guo, Y. Gao, K. Wang, and X. Liu, "Improved channel error calibration algorithm for azimuth multichannel SAR systems," *IEEE Geosci. Remote Sens. Lett.*, vol. 13, no. 7, pp. 1022–1026, Jul. 2016.

[22] A. Liu, G. Liao, L. Ma, and Q. Xu, "An array error estimation method for constellation SAR systems," *IEEE Geosci. Remote Sens. Lett.*, vol. 7, no. 4, pp. 731–735, Oct. 2010.

[23] L. Yan-Yang, Z. Li, S. Zhi-Yong, and Z. Bao, "A novel channel phase bias estimation method for spaceborne along-track multi-channel HRWS SAR in time-domain," in *Proc. IET Int. Radar Conf.*, 2013, pp. 1–4.

[24] S. Zuo, G. Sun, and M. Xing, "Improved channel error calibration method for the azimuth multichannel SAR," *J. Xidian Univ.*, vol. 44, no. 3, pp. 13–18, 2017.

[25] Y. Zhou et al., "A novel approach to doppler centroid and channel errors estimation in azimuth multi-channel SAR," *IEEE Trans. Geosci. Remote Sens.*, vol. 57, no. 11, pp. 8430–8444, Nov. 2019.

[26] Z. Li, Z. Bao, H. Wang, and G. Liao, "Performance improvement for constellation SAR using signal processing techniques," *IEEE Trans. Aerosp. Electron. Syst.*, vol. 42, no. 2, pp. 436–452, Apr. 2006.

[27] S.-X. Zhang et al., "Multichannel HRWS SAR imaging based on range-variant channel calibration and multi-doppler-direction restriction ambiguity suppression," *IEEE Trans. Geosci. Remote Sens.*, vol. 52, no. 7, pp. 4306–4327, Jul. 2014.

[28] G. Sun, J. Xiang, M. Xing, J. Yang, and L. Guo, "A channel phase error correction method based on joint quality function of GF-3 SAR dual-channel images," *Sensors*, vol. 18, no. 9, 2018.

[29] S.-X. Zhang, M.-D. Xing, X.-G. Xia, Y.-Y. Liu, R. Guo, and Z. Bao, "A robust channel-calibration algorithm for multi-channel in azimuth HRWS SAR imaging based on local maximum-likelihood weighted minimum entropy," *IEEE Trans. Image Process.*, vol. 22, no. 12, pp. 5294–5305, Dec. 2013.

[30] C. Jianlai and Y. Hanwen, "Wide-beam SAR autofocus based on blind rS," *Sci. China Inf. Sci.*, 2022, Art. no. 1674-733X.

[31] J. Chen, M. Xing, X. G. Xia, J. Zhang, B. Liang, and D. G. Yang, "SVD-based ambiguity function analysis for nonlinear trajectory SAR," *IEEE Trans. Geosci. Remote Sens.*, vol. 59, no. 4, pp. 3072–3087, Apr. 2021.

[32] G.-C. Sun, M. Xing, X.-G. Xia, Y. Wu, and Z. Bao, "Beam steering SAR data processing by a generalized PFA," *IEEE Trans. Geosci. Remote Sens.*, vol. 51, no. 8, pp. 4366–4377, Aug. 2013.

[33] H. Erdogan and J. A. Fessler, "Monotonic algorithms for transmission tomography," *IEEE Trans. Med. Imag.*, vol. 18, no. 9, pp. 801–914, Sep. 1999.

[34] T. J. Kragh, "Monotonic iterative algorithm for minimum-entropy autofocus," in *Proc. Adaptive Sensor Array Process. Workshop*, 2006.

[35] J. Hu, Y. Wang, and H. Li, "Phase error estimation and compensation for multi-channel SAR systems based on entropy minimization," *Acta Aeronautica Et Astronautica Sinica*, vol. 33, no. 10, pp. 1893–1904, 2012.

[36] D. G. Luenberger and Y. Ye, "Linear and nonlinear programming," *Int. Encyclopedia Social Behav.*, vol. 67, no. 2, pp. 8868–8874, 2004.

Jixiang Xiang (Member, IEEE) was born in Anyang, China, in 1994. He received the B.S. degree in communication engineering from the University of Electronic Science and Technology of China, Chengdu, China, in 2017. He is currently working toward the Ph.D. degree in signal processing with the National Laboratory of Radar Signal Processing, Xidian University, Xi'an, China.

His research interests include multichannel synthetic aperture radar (SAR) signal processing and SAR/groud moving targrt indicator.

Xiaojie Ding (Member, IEEE) was born in Xiaogan, China, in 1996. She received the B.S. degree in communication engineering from China Three Gorges University, Yichang, China, in 2019. She is currently working toward the master's degree in signal processing with the National Laboratory of Radar Signal Processing, Xidian University, Xi'an, China.

Her research interest includes multichannel SAR signal processing.

Guang-Cai Sun (Senior Member, IEEE) received the master's degree in communications engineering from Xi'an University of Posts and Telecommunications, Xi'an, China, in 2006, and the Ph.D. degree in signal and information processing from Xidian University, Xi'an, China, in 2012.

He is currently a Professor with the National Laboratory of Radar Signal Processing, and also with the Collaborative Innovation Center of Information Sensing and Understanding, Xidian University. He has authored or coauthored one book and published more than 50 papers. His research interests include imaging of several SAR modes, moving target detection, and imaging.

Zijing Zhang (Member, IEEE) was born in Beijing, China, in 1967. He received the B.S. and M.S. degrees in dynamics from the Harbin Institute of Technology, Harbin, China, in 1989 and 1992, respectively, and the Ph.D. degree in electrical engineering from Xidian University, Xi'an, China, in 2001.

From 2006 to 2006, he was a Visiting Scholar with The University of Manchester, Manchester, U.K. From 2016 to 2017, he was a Visiting Scholar with the University of Delaware, Newark, DE, USA. Since 1992, he has been with the National Laboratory of Radar Signal Processing, Xidian University, where he is a Professor. His research interests include radar signal processing and radar imaging.

Mengdao Xing (Fellow, IEEE) received the B.S. and Ph.D. degrees from Xidian University, China, in 1997 and 2002, respectively.

He is currently a Professor with the National Laboratory of Radar Signal Processing, Xidian University. He is also Associate Dean with the Academy of Advanced Interdisciplinary Research. He has written or cowritten more than 200 refereed scientific journal papers. He has also authored or coauthored two books about SAR signal processing. The total citation times of his research are greater than 8000. He was rated as one of Most Cited Chinese Researchers by Elsevier. He has achieved more than 40 authorized China patents. His current research interests include synthetic aperture radar, inversed synthetic aperture radar, sparse signal processing, and microwave remote sensing.

Dr. Xing's research was supported by various funding programs, such as, National Science Fund for Distinguished Young Scholars. He is currently an Associate Editor for radar remote sensing of IEEE TRANSACTIONS ON GEOSCIENCE AND REMOTE SENSING.

Wenkang Liu (Member, IEEE) was born in Dancheng County, China, in 1994. He received the B.S. degree in electronic information engineering from Xidian University (XDU), Xi'an, China, in 2015, and the Ph.D. degree in signal and information processing from the National Laboratory of Radar Signal Processing, XDU, in 2020 (with a focus on the imaging techniques of MEO/GEO SAR).

From 2019 to 2020, he was a visiting student with Naples University of "Parthenope," Naples, Italy. Since January 2021, he has been a Lecturer with Academy of Advanced Interdisciplinary Research, XDU. His research interests include novel space-borne radar system designing, SAR imaging algorithm development, and multipass SAR signal processing.